JOC The Journal of Organic Chemistry

Article

pubs.acs.org/joc

Tunneling Control: Competition between 6π-Electrocyclization and [1,5]H-Sigmatropic Shift Reactions in Tetrahydro-1*H*-cyclobuta[*e*]indene Derivatives

Sharmistha Karmakar and Ayan Datta*

Department of Spectroscopy, Indian Association for the Cultivation of Science, 2A and 2B Raja S. C. Mullick Road, Jadavpur, 700032 Kolkata, West Bengal, India

Supporting Information

ABSTRACT: Direct dynamics calculation using canonical variational transtition state theory (CVT) inclusive of small curvature tunneling (SCT) reveals the influential role of quantum mechanical tunneling (QMT) for 2,2a,5,7b-tetrahydro-1*H*-cyclobuta[*e*]indene derivatives (**2a−2j**) in governing their product selectivity. **2a−2j** follow two distinct reaction channels, namely, 6π-electrocyclization (**2** → **3**) and [1,5]H-sigmatropic shift (**2** → **4**), among which the activation barrier is higher for [1,5]H-shift (**2** → **4**), thereby favoring the kinetically controlled product (**3a−3j**) as anticipated. However, SCT calculations show that a narrower barrier and smaller mass of participating atoms make QMT more pronounced for [1,5]H-shift reaction despite its higher activation energy, which results in a competition between kinetic controlled (**2** → **3**) and tunneling controlled (**2** → **4**) products. At low temperature ($T \leq 170$ K), when QMT is the dominant pathway, the tunneling controlled product (**4a−4j**) is formed exclusively. As the reaction temperature increases, the role of QMT becomes less prominent and eventually gets kinetically controlled at room temperature. Nevertheless, QMT strongly tunes the product ratio at ambient temperatures by favoring the [1,5]H-shift reaction over 6π-electrocyclization. For **2a**, $k_{[1,5]\text{H-shift}}$:$k_{6\pi\text{-electrocyclization}}$ increases from 1:13 at CVT level to 1:2 at CVT+SCT level for room temperature.

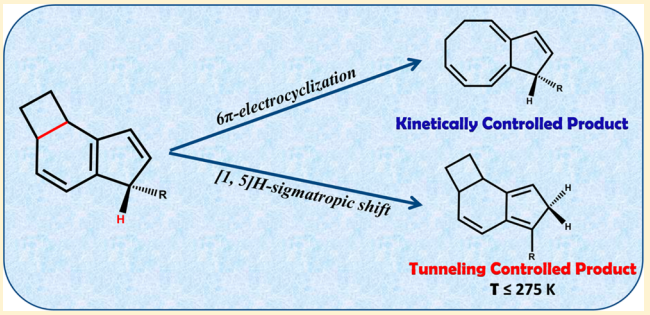

INTRODUCTION

Quantum mechanical tunneling (QMT) is a well-known physical phenomenon where a particle passes through a potential energy barrier rather than climbing over it.[1] Many chemical transformations like organic,[2−4] biomolecular[5,6] and catalytic processes[7,8] are known to have significant contribution from QMT, especially at low temperature. The signature of tunneling is most prominent for reactions like C−H insertion,[7,9] [1,2]H-shift in carbene,[10] [1,3] and [1,5]H-shift in aromatic and aliphatic systems[11−13] where the motion of light element, namely H atom is involved along the reaction coordinate. However, evidence for tunneling in heavy atom mediated transformations is comparatively rare. Examples of such processes are automerisation of cyclobutadiene,[14,15] rearrangement of cyclopropylcarbenes[16] and Myers−Saito cyclization of cyclic enyne-cumulene systems etc.[17,18] Deviation of Arrhenius plot from linearity and large kinetic isotope effect (KIE) cannot be explained without explicitly considering tunneling effects.[3] In the Eckart model, the effects of QMT are described as a correction factor to the classical rate where it usually does not change the fate of reaction.[19]

Nevertheless, there have recently been several examples in the literature which have shown that product formation is not governed by kinetic or thermodynamic criteria, but rather by the tunneling efficiency of the relevant parts of the molecule. This phenomenon is commonly referred to as tunneling control of chemical reactions.[20−24] [1,2]-shift of hydrogen in methylhydroxycarbene (**1a**) (see Scheme 1A) is one of the finest examples of tunneling control in chemical reactions. **1a** undergoes facile [1,2]H-tunneling along the C−O bond resulting thermodynamically stable product acetaldehyde at cryogenic temperature, although formation of vinyl alcohol is kinetically favorable.[21] Similarly for *tert*-butylhydroxycarbene the tunneling controlled product pivaldehyde is formed predominantly via [1,2]H-tunneling route over other kinetically preferred pathways.[22] Rearrangement of nor-adamantylmethylcarbene (**1b**) is also known to exhibit tunneling controlled product selectivity.[23]

Degenerate [3,3] Cope rearrangement of semibullvalene show strong signature of heavy atom tunneling making the reaction feasible even at cryogenic temperature.[25] Bicyclo[4.1.0]hepta-2,4-diene (norcaradiene) and bicyclo[4.2.0]octa-2,4-diene also possess similar structural feature like semibullvalene and rearrange to corresponding cycloheptatriene/cyclooctatriene via 6π-electrocyclization route.[26,27] Many phytochemicals such as endiandric acid and their derivatives[28,29] and metabolites like ocellapyrone A,[30] SNF4435 C

Received: November 17, 2016
Published: January 16, 2017

DOI: 10.1021/acs.joc.6b02759
J. Org. Chem. 2017, 82, 1558−1566

Scheme 1. (A) Some Examples of Reactions Showing Tunneling Controlled Product Selectivity; (B) Few Examples of Natural Products Capable of Undergoing 6π-Electrocyclization

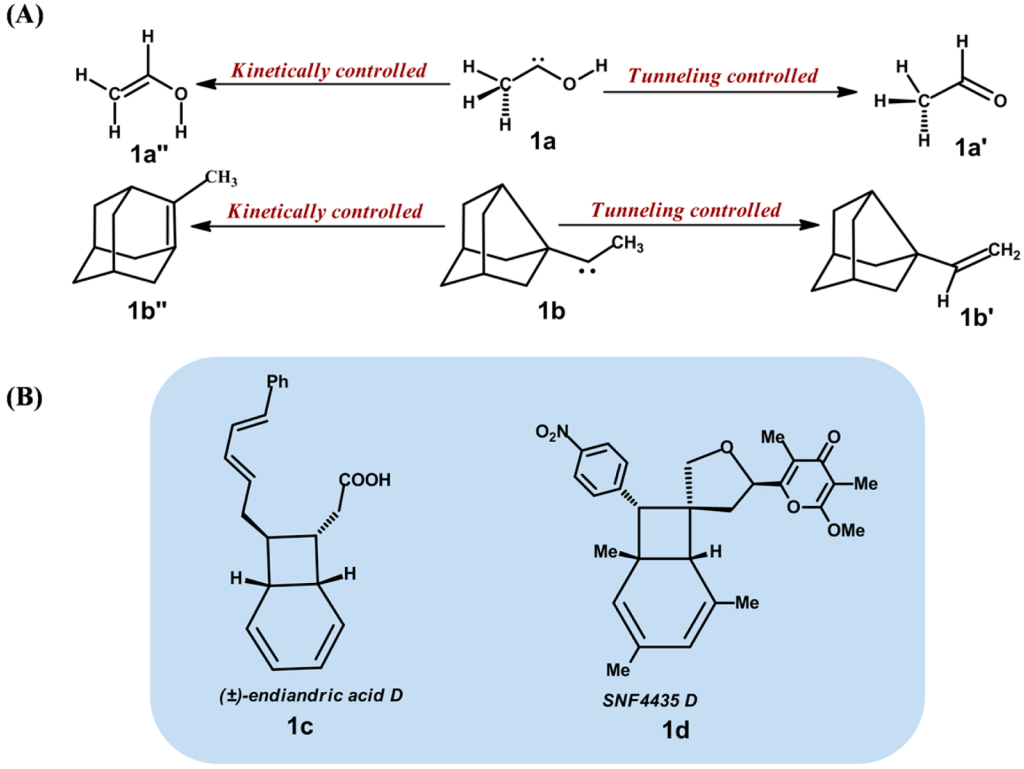

Scheme 2. 6π-Electrocyclization and [1,5]H-Sigmatropic Shift Reactions Considered in the Present Work (2a−2j)

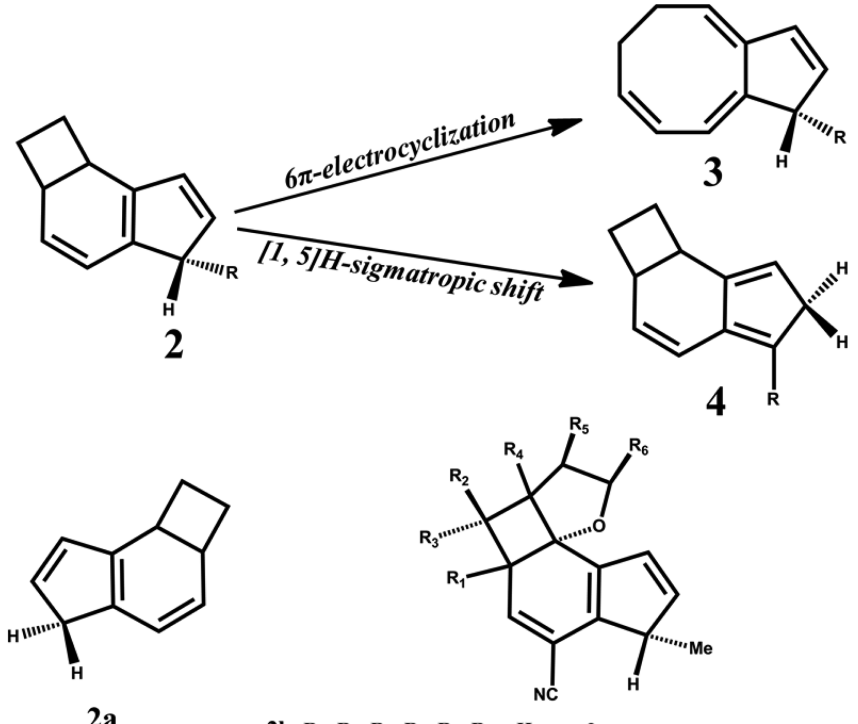

2b. $R_1, R_2, R_3, R_4, R_5, R_6 = H$
2c. R_1=Me, $R_2, R_3, R_4, R_5, R_6 = H$
2d. R_2=Me, $R_1, R_3, R_4, R_5, R_6 = H$
2e. R_4=Me, $R_1, R_2, R_3, R_5, R_6 = H$
2f. R_5=Me, $R_1, R_2, R_3, R_4, R_6 = H$
2g. R_1, R_2=Me, $R_3, R_4, R_5, R_6 = H$
2h. R_1, R_5=Me, $R_2, R_3, R_4, R_6 = H$
2i. R_3, R_6=Me, $R_1, R_2, R_4, R_5 = H$
2j. R_4, R_5=Me, $R_1, R_2, R_3, R_6 = H$

DOI: 10.1021/acs.joc.6b02759
J. Org. Chem. 2017, 82, 1558−1566

Table 1. Enthalpy of Activation, Free Energy of Activation (at 298.15 K) in kcal/mol and the Characteristics Imaginary Frequency (ν_i) in cm^{-1} of the Transition State for 2a Calculated at Various DFT Levels for 6π-Electrocyclization and [1,5]H-Sigmatropic Shift Reactions

	6π-electrocyclization			[1,5]H-sigmatropic shift		
	$\Delta H^{\ddagger}$	$\Delta G^{\ddagger}$	ν_i	$\Delta H^{\ddagger}$	$\Delta G^{\ddagger}$	ν_i
B3LYP/6-31+G(d,p)	24.1 (23.4)[a]	24.6 (24.0)[a]	513i (520i)[a]	25.6 (25.4)[a]	26.1 (25.9)[a]	1262i (1237i)[a]
BPW91/6-31+G(d,p)	22.1	22.6	457i	22.5	23.1	1176i
BLYP/6-31+G(d,p)	19.5	20.0	462i	24.7	25.2	1250i
M062X/6-31+G(d,p)	28.1	28.5	544i	23.6	24.1	1144i
ωB97XD/6-31+G(d,p)	30.3	30.8	565i	25.4	25.9	1227i
MPW1K/6-31+G(d,p)	31.3	31.7	568i	25.0	25.5	1217i
CBS-QB3	24.3	24.8	520i	25.8	26.3	1263i

[a]Computed using B3LYP/aug-cc-pVTZ level of theory.

and SNF4435 D[31,32] (see Scheme 1B) display fascinating structural diversity, where the basic ring structure of bicyclo[4.2.0]octa-2,4-diene is common to all. Wide structural variety in these natural products leads to numerous biological activities such as antibacterial, anticancer and antitubercular properties.[31,33] Synthesis of these biologically relevant molecules can be achieved via 8π−6π electrocyclization cascade of substituted 1,3,5,7-tetracene or through photoinduced intramolecular [2+2] cycloaddition of alkene moiety to the substituted benzene.[28,29,32,34] While norcaradiene shows facile ring rearrangement the bicyclo[4.2.0]octa-2,4-diene analog possess substantial barrier. Presence of an additional [1,5]H-sigmatropic shift channel with these set of compounds opens up the possibility of H-shift reaction.[13] Hence, it is possible to tune the barrier heights and widths to create a situation where [1,5]H-shift and 6π-electrocyclization competes. Tunneling by H atom as expected in [1,5]H-shift is more favorable than C-tunneling in 6π-electrocyclization, a purely mass effect, provided the barrier is not too large.[1]

In this manuscript, we have modeled a system where a cyclopentene moiety is being attached with the bicyclo[4.2.0]-octa-2,4-diene core (see Scheme 2) such that one part is capable of undergoing [1,5]H-sigmatropic shift while the other one for 6π-electrocyclization. We have considered 2,2a,5,7b-tetrahydro-1*H*-cyclobuta[*e*]indene (**2a**) and derivatives of **2a** as model systems for detailed calculations. A rich variety of natural products primarily fungal metabolites, e.g., protoilludane and punctaporonane, possess an annulated 5/6/4-ring system similar to **2a** and they exhibit diverse structural variety with different substitution patterns.[35] Synthesis of these natural products (protoilludanes and related sesquiterpenes) is well documented in the past literature by several efficient methods.[36] As our studied systems (**2a−2j**) resemble closely with these biologically active molecules, hence it is highly possible to synthesis **2a** and its derivatives by similar techniques. On the basis of direct dynamics calculations followed by small curvature tunneling (SCT) approximation we find that the fate of reaction is strongly controlled by QMT effects, which are evident in their product ratios. For example, while the $k_{6\pi\text{-electrocyclization}}$:$k_{[1,5]\text{H-shift}}$ = 13:1 for **2a** without tunneling at 300 K reduces to 2:1 with tunneling. Interestingly the product selectivity changes entirely at lower temperature (T = 220 K) due to tunneling for which at CVT+SCT, the $k_{6\pi\text{-electrocyclization}}$:$k_{[1,5]\text{H-shift}}$ = 1:46, while without tunneling it is 33:1. In the following sections, we discuss the computational details, results and conclusions.

COMPUTATIONAL DETAILS

All the electronic structure calculations for 6π-electrocyclization and [1,5]H-sigmatropic shift in **2a−2j** were carried out using the hybrid B3LYP functional within density functional theory (DFT).[37,38] The B3LYP functional has been shown to provide an accurate estimate for barrier heights and reaction energies in 6π-electrocyclization and [1,5]H-shift reactions previously.[39−44] The 6-31+G(d,p) basis set was employed.[45] Additional calculations at various others level of theory were also carried to verify the suitability of the B3LYP functional for those transformations. Harmonic frequencies calculations ensure that reactants and products are at local minima while transition states (TS) are first order saddle points. All the calculations were performed at the closed shell singlet potential energy surface as no spin contamination was observed in unrestricted wave function level. The rate constants for classical over the barrier transformations were obtained using canonical variational transition state (CVT) theory.[46] The effect of multidimensional tunneling on the classical rate equations were incorporated through small curvature tunneling (SCT) approximation.[47,48] Direct dynamics calculations were performed using GAUSSRATE[49] as the interface between Gaussian 09[50] and POLYRATE.[51] The vibrational levels of reactant were treated by harmonic approximation. The reorientation of the dividing surface (RODS) algorithm has been employed to get an accurate free energy surface.[52]

RESULTS AND DISCUSSION

Since all the studied systems are capable of undergoing 6π-electrocyclization and [1,5]H-sigmatropic reactions simultaneously, one need to select a density functional which can describe both the processes on an equal footing in terms of chemical accuracy. Table 1 lists the computed barriers and the characteristics imaginary frequency of the transtition state for **2a** at various density functional namely B3LYP, BPW91, BLYP, M062X, ωb97xD and MPW1K at the 6-31+G(d,p) basis set level. We have also calibrated the computed activation barrier using higher CBS-QB3 level of theory. As tabulated in Table 1 that the B3LYP functional favors the 6π-electrocyclization reaction by $\Delta G^{\ddagger}$ = 1.5 kcal/mol and so does the pure DFT functional, BLYP ($\Delta\Delta G^{\ddagger}$ = 5.2 kcal/mol). On the contrary, the M062X and ωb97xD functionals determine a reverse trend in product distribution by favoring the H-shift reaction over 6π-electrocyclization. Previous literature suggests that the MPW1K and B3LYP functionals provide accurate description of the activation barriers for [1,5]H-shift reactions for cyclopentadiene and *Z*-1,3-pentadiene derivatives though the MPWIK functional seems to describe tunneling corrections better.[13,44] However, the MPW1K functional is found to overestimate the barrier for 6π-electrocyclization. On the other hand, the B3LYP functional has been shown to reproduce the experimental

DOI: 10.1021/acs.joc.6b02759
J. Org. Chem. 2017, 82, 1558−1566

Table 2. Free Energy of Activation and Reaction Free Energy (at 298.15 K) in kcal/mol Calculated at B3LYP/6-31+G(d,p) Level of Both the Reactions for 2a−2j

		$\Delta G^{\ddagger}$	ΔG			$\Delta G^{\ddagger}$	ΔG
2a	**2a → 3a**	24.6	−0.6	**2f**	**2f → 3f**	17.7	−0.2
	2a → 4a	26.1	−1.7		**2f → 4f**	24.6	−1.9
2b	**2b → 3b**	17.9	−0.3	**2g**	**2g → 3g**	19.0	+0.6
	2b → 4b	24.6	−2.4		**2g → 4g**	21.3	−6.4
2c	**2c → 3c**	16.8	+2.1	**2h**	**2h → 3h**	16.7	−3.5
	2c → 4c	22.1	−5.4		**2h → 4h**	22.9	−4.5
2d	**2d → 3d**	20.7	+3.7	**2i**	**2i → 3i**	17.2	+0.2
	2d → 4d	24.4	−4.9		**2i → 4i**	24.9	−1.6
2e	**2e → 3e**	18.0	+2.5	**2j**	**2j → 3j**	17.6	+1.9
	2e → 4e	24.8	−2. 0		**2j → 4j**	24.7	−1.6

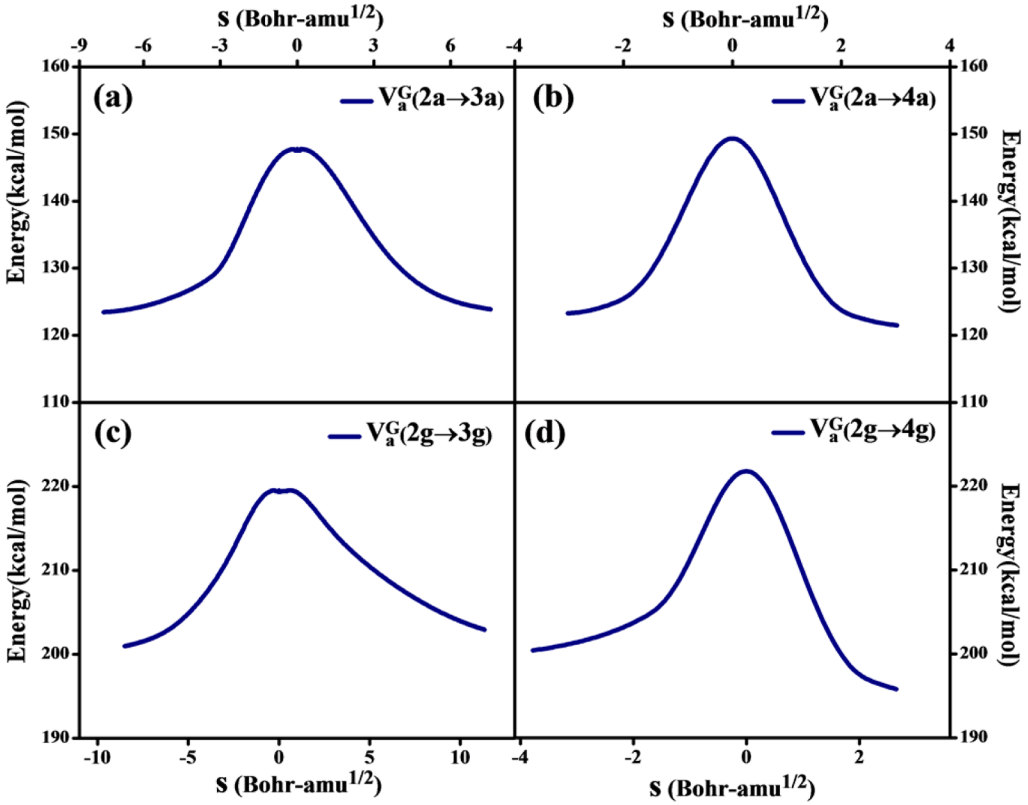

Figure 1. Profile of V_a^G for (a) **2a** → **3a**, (b) **2a** → **4a**, (c) **2g** → **3g** and (d) **2g** → **4g**.

reaction barriers reliably for several pericyclic reactions including 6π-electrocyclization in bicyclo[4.2.0]octa-2,4-diene derivatives.[25,39−43,53] Fry has investigated valence tautomerization in a series of substituted 1,3,5-cyclooctatriene into the corresponding bicyclooctadienes and it can be found that B3LYP/6-31G(d) level of theory reasonably reproduce the experimental barrier and reaction energy for 1,3,5-cyclooctatriene (**5a**) (see Scheme S1 in Supporting Information).[43] Although they recommended CBS-QB3 level of theory as the superior choice for these set of compounds, high computational cost restricts its application. Our model systems resembles their studied system (**5a′**) closely where the bicyclo[4.2.0]octa-2,4-diene core is common to all of them. Therefore, we have calculated the reaction barriers and energies for **2a** using CBS-QB3 level of theory to verify the performance of different density functionals. Our results suggest that (see Table 1) B3LYP functional along with 6-31+G(d,p) basis set gives an excellent agreement with higher CBS-QB3 level of theory, on the other hand improvement in basis set has little effect in their relative barrier height difference between two competitive reaction steps (see Table 1 and Table S1 in SI). Similarity of CBS-QB3 results with B3LYP functional in **2a** encourage us to select the cost efficient B3LYP functional along with 6-31+G(d,p) basis set to study the competition between [1,5]H-shift and 6π-electrocyclization in **2a−2j** and it is found to be capable to describe both the processes. Choice of an uniform DFT functional ensures that absolute errors in estimation of barriers would be hopefully canceled out while comparing the relative rates of [1,5]H-shift and 6π-electrocyclization.

2,2a,5,7b-Tetrahydro-1*H*-cyclobuta[*e*]indene and derivatives of **2a** with varying substitution pattern (**2a−2j**) follow two different reaction pathways producing two distinct set of products, namely **3** and **4** (see Scheme 2). The relative product ratio of two competitive reactions is primarily governed by their differences in barriers at the reaction temperature.[54] A difference in barrier energies of 1 kcal/mol between two

DOI: 10.1021/acs.joc.6b02759
J. Org. Chem. 2017, 82, 1558−1566

Table 3. CVT, CVT+SCT Rate Constants (in s^{-1}) and Tunneling Transmission Coefficient (κ_{SCT}) Calculated at B3LYP/6-31+G(d,p) Level for 2a → 3a and 2a → 4a at T = 100, 150, 200, 240, 275, and 300 K

	2a → 3a			2a → 4a		
T (K)	k_{CVT}	$k_{CVT+SCT}$	κ_{SCT}	k_{CVT}	$k_{CVT+SCT}$	κ_{SCT}
100	1.32×10^{-41}	1.14×10^{-38}	8.63×10^{2}	5.18×10^{-45}	1.41×10^{-14}	2.72×10^{30}
150	8.74×10^{-24}	2.87×10^{-23}	3.29	4.97×10^{-26}	1.85×10^{-13}	3.72×10^{12}
200	7.58×10^{-15}	1.37×10^{-14}	1.80	1.61×10^{-16}	1.52×10^{-11}	9.45×10^{4}
240	2.30×10^{-10}	3.41×10^{-10}	1.48	9.29×10^{-12}	2.04×10^{-09}	2.20×10^{2}
275	1.67×10^{-07}	2.24×10^{-07}	1.34	1.00×10^{-08}	2.26×10^{-07}	22.5
300	7.21×10^{-06}	9.21×10^{-06}	1.28	5.46×10^{-07}	5.41×10^{-06}	9.90

parallel reactions should lead to product preference of 85%, while a product ratio of 99:1 is anticipated when the differences in barriers is ≥3 kcal/mol at 300 K. This scenario, though valid in most cases, becomes increasingly divergent for reactions where contribution of tunneling is significant.[21] Within the tunneling regime, the classical rate constants get enhanced by several orders of magnitude. The extent of QMT primarily depends on the reaction barrier, mass of particle and the width of the barrier.[1] In the present case, between these two competitive reaction channels, one involves the shift of H atom forming **4** while the other one involves the motion of carbon atom along the reaction coordinate producing **3**. Therefore, it is expected that tunneling will be more pronounced for the [1,5]H-shift reaction.

As can be seen from Table 2 that the free energy barrier for 6π-electrocyclization in **2a** (**2a** → **3a**) is 1.5 kcal/mol lower than for the corresponding [1,5]H-shift reaction (**2a** → **4a**). This is in agreement with the CVT product ratio of 92:8 between **3a** and **4a** at 300 K. For **2b**, the activation barrier for electrocyclization selectively decreases considerably. The presence of electron withdrawing groups are known to activate the electrocyclization reaction,[55] and this is also evident for **2b** for which the introduction of a −CN group at the cyclohexadiene moiety and attachment of oxygenated five membered ring lowers the **2b** → **3b** barrier with respect to **2a**. In case of **2b**, the $\Delta\Delta G^{\ddagger} = \Delta G^{\ddagger}(\mathbf{2b} \rightarrow \mathbf{4b}) - G^{\ddagger}(\mathbf{2b} \rightarrow \mathbf{3b}) =$ 6.7 kcal/mol and hence, the electrocyclized product, **3b** will be formed exclusively at all temperature. Substitution by −Me groups at various position of **2b** ranging from R_1 to R_6 leads to different derivatives of **2b** namely **2c**−**2j** (see Scheme 2). Presence of a single −Me group at R_1, R_4 and R_5 has inconsequential effect on the reaction barriers. However, −Me group at R_2 increase the electrocyclization barrier by 2.8 kcal/mol. Introduction of another −Me group results in four different isomers namely **2g**−**2j**. The activation barrier for [1,5]H-sigmatropic shift remains unchanged within the whole series (**2b**−**2j**) except for **2c**, **2g** and **2h**, for which the barriers decrease by ∼2 kcal/mol. The difference in free energy barrier between the two reactions pathways varies from 1.5 kcal/mol to 7.7 kcal/mol. The lowest $\Delta\Delta G^{\ddagger}$ = 1.5 and 2.1 kcal/mol correspond to **2a** and **2g**. We have performed direct dynamics calculations for these two systems (**2a** and **2g**) as $\Delta\Delta G^{\ddagger} \approx 2$ kcal/mol is quite amenable to be tuned by QMT effects which should be observed in their relative product distribution at $T \geq$ 200 K. Both the reactions are mildly exergonic with ΔG(**2a** → **3a**) = −0.6 kcal/mol and ΔG(**2a** → **4a**) = −1.7 kcal/mol. In the case of **2g**, while [1,5]H-shift is exergonic (ΔG(**2g** → **4g**) = −6.4 kcal/mol), electrocyclization is mildly endergonic with ΔG(**2g** → **3g**) = +0.6 kcal/mol.

An accurate description of molecular potential energy surface (PES) is highly desirable for computing reliable rate of reaction through direct dynamics calculation. In Figure 1 we represent the profile of the ground state vibrational adiabatic potential energy curve [$V_a^G(s)$] along the reaction coordinate (s in Bohr-amu$^{1/2}$) for **2a** → **3a**, **2a** → **4a**, **2g** → **3g** and **2g** → **4g** and the variation of classical potential energy [$V_{MEP}(s)$] with the reaction coordinate is given in the Supporting Information (see Figure S1). The $V_{MEP}(s)$ curve represents the change in electronic energy along the minimum energy path(MEP), while the profile for $V_a^G(s)$ can be obtained by correcting the V_{MEP} curve by including zero point energy (ZPE) as $V_a^G(s) = V_{MEP}(s)$ + ZPE(s).[48]

For all the cases the profile of $V_a^G(s)$ profile resembles the $V_{MEP}(s)$ curve as the variation in ZPE(s) along the reaction coordinate is negligible. The representative tunneling energy (RTE) is the energy below the top of barrier where the probability of tunneling is maximum at a particular temperature.[48] In case of **2a**, the maximum vibrational adiabatic potential is 147.7 kcal/mol for **2a** → **3a** and 149.3 kcal/mol for **2a** → **4a**. The corresponding RTE values lie 0.1 and 14.8 kcal/mol below the top of barrier respectively at 220 K. Likewise for **2g**, the maxima on the V_a^G surfaces appear at 219.5 and 221.8 kcal/mol for **2g** → **3g** and **2g** → **4g** respectively. The RTE found to be 1.6 and 11.4 kcal/mol below the highest point in V_a^G at 220 K for **2g** → **3g** and **2g** → **4g** respectively. Note that H atom tunneling in **2a** → **4a** and **2g** → **4g** occur far below the top of the barrier compared to C-tunneling in **2a** → **3a** and **2g** → **3g** due to facile tunneling.

The $V_a^G(s)$ profile of the electrocylization reactions for **2a** → **3a** and **2g** → **3g** appear to be much wider compared to the H-sigmatropic shift. For example, the $V_a^G(s)$ curves span over a large s range of −11 Bohr-amu$^{1/2}$ to 9 Bohr-amu$^{1/2}$. However, in case of [1,5]H-shift reactions for **2a** → **4a** and **2g** → **4g**, the adiabatic potential curve is found to be significantly narrower and range from s = −3 Bohr-amu$^{1/2}$ to 3 Bohr-amu$^{1/2}$. This is also evident from the magnitude of imaginary frequency (ν_i) of the reactive mode. For **2a** → **3a** and **2g** → **3g**, the ν_i are 513 and 380 cm^{-1} while for **2a** → **4a** and **2g** → **4g** they are 1262 cm^{-1}and 1220 cm^{-1} respectively. Higher frequency for the reactive mode indicates a narrower barrier in **2a** → **4a** and **2g** → **4g**; hence, the [1,5]H-shift reactions possess a relatively higher yet thinner barrier compared to its competitive ring opening step (**2** → **3**). A narrower barrier coupled with the lighter mass of H atom should facilitate [1,5]H-shift reactions more than 6π-electrocyclization reactions.

Table 3 lists the CVT and CVT + SCT rate constants and tunneling transmission coefficient (κ_{SCT}) for 6π-electrocyclization and [1,5]H-sigmatropic shift reactions in **2a** at six representative temperatures (T = 100, 150, 200, 240, 275, and 300 K). The CVT rate constants for **2a** → **3a** are larger than that of **2a** → **4a** anticipated from their differences in barrier energies. The calculated E_a^{CVT}(**2a** → **4a**) − E_a^{CVT}(**2a** →

DOI: 10.1021/acs.joc.6b02759
J. Org. Chem. 2017, 82, 1558−1566

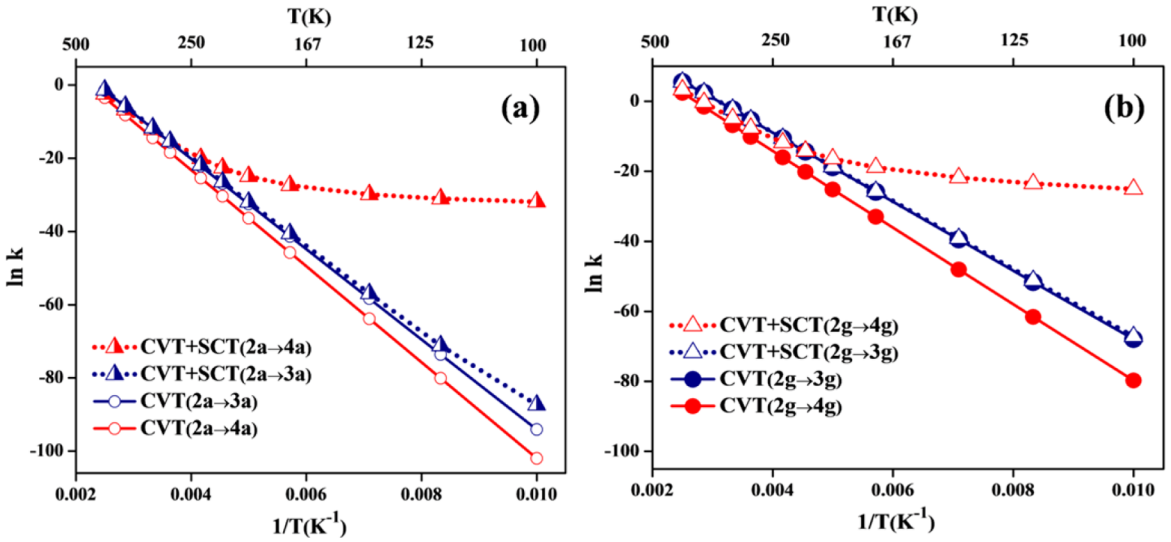

Figure 2. Arrhenius plots of the CVT and CVT+SCT rate constants for (a) **2a** and (b) **2g** from 100 to 400 K.

Table 4. CVT, CVT+SCT Rate Constants (in s^{-1}) and Tunneling Transmission Coefficient (κ_{SCT}) Calculated at B3LYP/6-31+G(d,p) Level for 2g → 3g and 2g → 4g at T = 100, 150, 200, 240, 275, and 300 K

	2g → 3g			2g → 4g		
T (K)	k_{CVT}	$k_{CVT+SCT}$	κ_{SCT}	k_{CVT}	$k_{CVT+SCT}$	κ_{SCT}
100	3.13×10^{-30}	6.79×10^{-30}	2.27	2.39×10^{-35}	1.27×10^{-11}	5.31×10^{23}
150	4.78×10^{-16}	6.32×10^{-16}	1.37	1.42×10^{-19}	7.21×10^{-10}	5.07×10^{9}
200	6.43×10^{-09}	7.44×10^{-09}	1.18	1.18×10^{-11}	7.46×10^{-08}	6.33×10^{3}
240	2.45×10^{-05}	2.69×10^{-05}	1.12	1.11×10^{-07}	7.45×10^{-06}	67.25
275	4.72×10^{-03}	5.06×10^{-03}	1.09	3.79×10^{-05}	4.85×10^{-04}	12.8
300	9.60×10^{-02}	1.02×10^{-01}	1.08	1.07×10^{-03}	7.35×10^{-03}	6.86

3a)= 1.54, 1.44, and 1.45 kcal/mol at T = 100, 200 and 300 K, respectively and CVT E_a show only a 0.1 kcal/mol variation in the temperature range (T = 100−300 K). This is also observed from the Arrhenius plots in Figure 2a for which the CVT rates for **2a** → **4a** lie below that of **2a** → **3a** rates in the entire temperature range. The calculated ratio of CVT rate constants [k_{CVT}(**2a** → **3a**)/k_{CVT}(**2a** → **4a**)] turns out to be 2500, 16.7, and 13.2 at T = 100, 275 and 300 K, respectively, thereby indicating that **3a** is the major product with product yield of >90%.

Inclusion of tunneling enhances the overall rate for both **2a** → **3a** and **2a** → **4a** at all temperatures. However, in case of **2a** → **4a** the increase is much more prominent. For example, at 100 K, **2a** → **4a** has ~10^{30} fold enhancement whereas for **2a** → **3a** it is only ~10^{2} times. The tunneling probability (T) for a particular reaction can be approximately written as $T = e^{-w\sqrt{V_0 m}}$, where V_0 and w are the barrier height and width and m signifies mass of moving particle.[1] Hence, in case of **2a** → **4a**, a narrow barrier and smaller mass of moving particle supersedes the effect of marginally larger barrier resulting in much more efficient tunneling by hydrogen vis-à-vis **2a** → **3a**. Clearly QMT not only increases the rate of the reactions but also alters the preference for product formation from **3a** (*kinetically controlled product*) to **4a** (*tunneling controlled product*), at least at lower T. At 100 K, $k_{CVT+SCT}$(**2a** → **4a**) ≫ $k_{CVT+SCT}$(**2a** → **3a**) by a factor of ~10^{24}. With increase in temperature, the over the barrier process becomes increasingly favorable which causes a gradual decrease of transmission probability κ_{SCT}. At 275 K, $k_{CVT+SCT}$(**2a** → **4a**) equals $k_{CVT+SCT}$(**2a** → **3a**) and as temperature increases, the $k_{CVT+SCT}$(**2a** → **3a**) exceeds $k_{CVT+SCT}$(**2a** → **4a**).The difference between the activation energies, $\Delta E_a^{CVT+SCT} = E_a^{CVT+SCT}$(**2a** → **4a**) − $E_a^{CVT+SCT}$(**2a** → **3a**), are 15.34, 15.3, and 2.64 kcal/mol at T = 100, 200 and 300 K respectively. The ratio of CVT+SCT rate constants, $k_{CVT+SCT}$(**2a** → **3a**)/$k_{CVT+SCT}$(**2a** → **4a**) are 8 × 10^{-25}, 9 × 10^{-4} and 1.70 at T = 100, 200 and 300 K respectively. Clearly at low T, when QMT is the dominant pathway the tunneling controlled product **4a** is formed despite its higher barrier. At higher temperatures (T > 275 K), tunneling does not completely control the product formation though it significantly modifies the product distribution. Manifestation of this effect is also observed in Figure 2a where the CVT+SCT Arrhenius plot for **2a** → **4a** lies above **2a** → **3a** up to T ~ 275 K before eventually falling below it.

In case of **2g**, the rate for both **2g** → **3g** and **2g** → **4g** transformations increases due to lower activation barrier compared to **2a** (see Table 4). For **2g**, the difference in energies between **2g** → **4g** and **2g** → **3g** is higher by 0.7 kcal/mol compared to **2a**. Their differences in E_a^{CVT}(**2g** → **4g**) − E_a^{CVT}(**2g** → **3g**) are 2.2, 2.1, and 2.1 kcal/mol at 100, 200, and 300 K respectively. A difference of E_a^{CVT} by ~2 kcal/mol leads to k_{CVT}(**2g** → **3g**) > k_{CVT}(**2g** → **4g**) irrespective of temperature, with a preference of >90% for electrocyclization. The ratio of CVT rates, k_{CVT}(**2g** → **3g**)/k_{CVT}(**2g** → **4g**), are 1.3 × 10^{5}, 5.4 × 10^{2} and 89.7, which the same at the CVT+SCT level are 5.3 × 10^{-19}, 0.1 and 13.9 at T = 100, 200, and 300 K respectively. The CVT rates indicate a clear preference of the kinetically controlled product, **3g** over **4g** at all temperatures. However, inclusion of tunneling changes the fate of product formation and exclusively prefers **4g**, the tunneling controlled

DOI: 10.1021/acs.joc.6b02759
J. Org. Chem. 2017, 82, 1558−1566

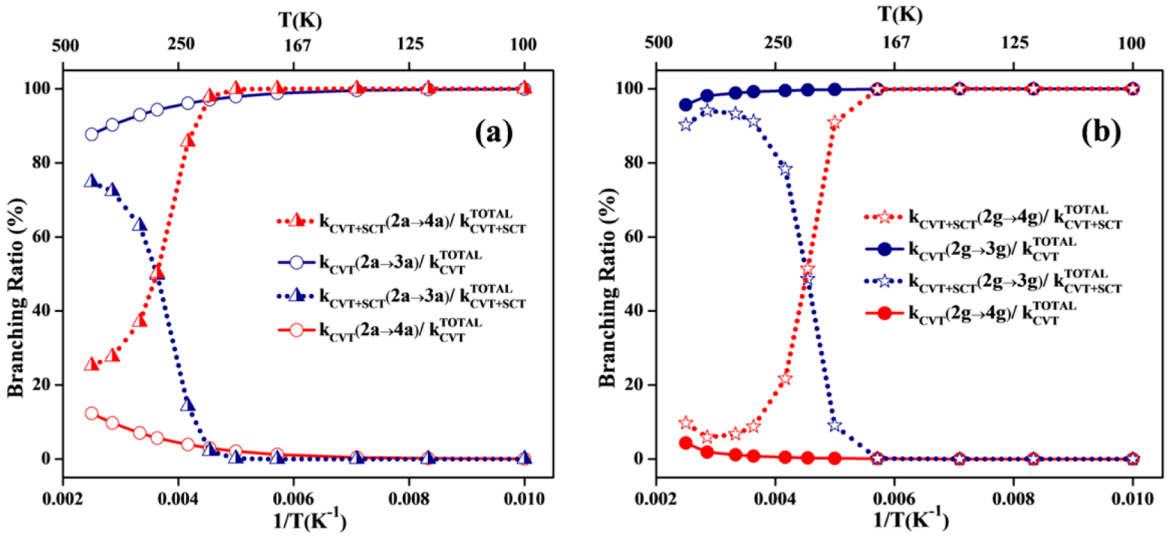

Figure 3. Temperature variation of the branching ratio for the CVT and CVT+SCT rate constants in (a) **2a** and (b) **2g** from 100 to 400 K.

product at lower temperatures. With rise in temperature, the relative population of **3g** increases as the contribution from QMT becomes less significant. In the case of **2g**, the crossover occurs at ∼220 K and the $k_{CVT+SCT}$ rates are 6.46 × 10^{-7} s^{-1} and 6.83 × 10^{-7} s^{-1} for **2g** → **3g** and **2g** → **4g** respectively. Figure 2b represents the Arrhenius plot of CVT and CVT +SCT rates for **2g** → **3g** and **2g** → **4g** in the temperature range T = 100−400 K. The Arrhenius plots for **2g** also show similar behavior as that for **2a** with the CVT profile for **2g** → **3g** always above the **2g** → **4g** and the CVT+SCT curve for **2g** → **4g** lying above the **2g** → **3g** up to T ∼ 220 K before crossing it. Although QMT alters the preferred product formation from **3a**/**3g** to **4a**/**4g** by selectively enhancing the H-shift rate at low temperature; still the predicted rate constants are far below than the experimentally detectable regime. However, at elevated temperatures (T > 220 K), tunneling alongwith thermal activation modify the rate constants in such a way that it might be measured experimentally and a significant change in the product ratio from its CVT value would serve as fingerprints of tunneling at ambient temperature.

Branching ratio is an important experimental observable for reactions with multiple product channels. For a parallel reaction it can be described as the fraction of individual rate constant to the total rate. At a particular temperature; $k_{CVT/CVT+SCT}(2 \rightarrow 3)/k^{TOTAL}_{CVT/CVT+SCT}$ and $k_{CVT/CVT+SCT}(2 \rightarrow 4)/k^{TOTAL}_{CVT/CVT+SCT}$ represent the CVT and CVT+SCT branching ratios for **3** and **4** respectively. The temperature dependence of branching ratios (in percentages) for **3a**, **4a** and **3g**, **4g** are plotted in Figure 3a and Figure 3b, respectively.

Figure 3 shows that the CVT plots of branching ratio for **3a**, **3g** and **4a**, **4g** which remain nearly constant with temperature. At $T \leq$ 100−175 K the calculated CVT branching ratios for **3a** and **3g** are ∼98−100%, which decrease marginally with increase in temperature and reach 85−95% at T ∼ 400 K. Therefore, classically the kinetically controlled products **3a** and **3g** are formed almost entirely up to T ∼ 400 K. However, the CVT +SCT plots for **4a** and **4g** show an entirely different behavior. They reach a maximum (∼100%) at low temperature ($T \leq$ 100−160 K) and then gradually decrease and cross the CVT +SCT curve of **3a** and **3g** at T = 275 and 220 K respectively. At low temperature ($T \leq$ 100−170 K) when the reactants do not possess enough energy to overcome the potential energy barrier, the product formation is governed by tunneling and the tunneling controlled products **4a** and **4g** are formed exclusively. At T > 170 K, as the reactants acquire more thermal energy, the relative population of **3a** and **3g** get increased although **4a** and **4g** still are the major products up to T = 275 and 220 K respectively. The effects of QMT get slowly diminished at higher temperatures resulting in **3a** and **3g** as the major products. Nevertheless, the product ratios for **4a** and **4g** get improved significantly compared to CVT results at relatively higher temperature. At 300 K, the calculated CVT product ratios for **3a**:**4a** and **3g**:**4g** are 93:7 and 99:1 respectively, which gets modified to 63:37 and 93:7 at CVT+SCT level.

CONCLUSION

In summary, on the basis of calculations for model systems, comprising both [1,5]H-sigmatropic unit and 6π-electrocyclization moiety, we show that though the barrier for H-shift reaction is higher compared to the electrocylization step in the whole series (**2a**−**2j**), QMT effects are more important for them. Rate constant calculations inclusive of small curvature tunneling reveal the influential role of QMT for **2a** and **2g** in governing the product selectivity. A narrower barrier and smaller mass of moving particle compensate its higher barrier, resulting in a more pronounced tunneling effect for H-shift reactions, namely **2a** → **4a** and **2g** → **4g**. This is also apparent from the curvature of CVT+SCT Arrhenius plots. **2a** and **2g** represent new example of chemical reaction where the tunneling controlled products **4a** and **4g** are formed exclusively at low temperature (up to T ∼ 170 K). The fraction of kinetically controlled products, **3a** and **3g** get enhanced gradually as reactant accumulate more thermal energy upon at higher temperatures, although **4a** and **4g** are still the major products up to T ∼ 220−270 K with a detectable rate constant. At further higher temperatures, the effects of tunneling decay rapidly, resulting **3a** and **3g** as the major products. The present work demonstrates that a difference in activation barrier between two competitive reaction channels cannot entirely dictate the product ratios. Tunneling effects can in-fact modify the product preferences significantly or even reverse them at ambient temperatures. Hence, for parallel reactions with comparable barriers, the possibility of tunneling control should be explored, particularly if the barrier is narrow or the particles

DOI: 10.1021/acs.joc.6b02759
J. Org. Chem. 2017, 82, 1558−1566

are not too heavy. Our prediction can be verified experimentally by measuring the relative product ratio of two competitive reaction channels with varying temperatures (low to high). Performing a product distribution analysis at even a single temperature (T = 300 K) would provide evidence for QMT. For example, we predict a much larger fraction of the H-shift product compared to the 6π-electrocyclization (1:2) as a result of tunneling than that based on solely kinetic consideration (1:12) at room temperature. This would be a simple yet strong experimental test for our predictions. It has not escaped our attention that under physiological conditions (both in vivo and in vitro) multiple reactions involving H atom or proton compete with each other and tunneling might be an important key for understanding the preference of one over others.

■ ASSOCIATED CONTENT

Supporting Information

The Supporting Information is available free of charge on the ACS Publications website at DOI: 10.1021/acs.joc.6b02759.

Optimized geometries, energies, thermal corrections, entropy corrections and harmonic frequencies for **2a**−**2j** and the transition structure connecting them, 6π-electrocyclization scheme in 1,3,5-cyclooctatriene, reaction energy and barrier for **2a** using different basis set, reaction energies and barriers for **2a**−**2j** at B3LYP/6-31+G(d,p), profile of V_{MEP} for **2a** and **2g**, CVT, CVT + SCT rate constants and branching ratios from 100 to 400 K for **2a** and **2g**, the complete lists of authors for refs 48 and 49 (PDF)

■ AUTHOR INFORMATION

Corresponding Author

*E-mail: spad@iacs.res.in.

ORCID

Ayan Datta: 0000-0001-6723-087X

Notes

The authors declare no competing financial interest.

■ ACKNOWLEDGMENTS

S.K. thanks CSIR India for SRF. A.D. thanks DST, BRNS, and INSA for partial funding. The authors thank the IACS CRAY supercomputer for computational resources.

■ REFERENCES

(1) Bell, R. P. *The Tunnel Effect in Chemistry*; Chapman and Hall: London, 1980.
(2) Patureau, F. W. *Angew. Chem., Int. Ed.* **2012**, *51*, 4784−4786.
(3) Kaestner, J. *WIREs Comput. Mol. Sci.* **2014**, *4*, 158−168.
(4) Ley, D.; Gerbig, D.; Wagner, J. P.; Reisenauer, H. P.; Schreiner, P. R. *J. Am. Chem. Soc.* **2011**, *133*, 13614−13621.
(5) Pu, J.; Gao, J.; Truhlar, D. G. *Chem. Rev.* **2006**, *106*, 3140−3169.
(6) Scrutton, N. S. *Quantum Tunnelling in Enzyme-Catalysed Reactions*; Royal Society of Chemistry, 2009.
(7) Khanh Mai, B.; Kim, Y. *Chem. - Eur. J.* **2013**, *19*, 3568−3572.
(8) Moiseyev, N.; Rucker, J.; Glickman, M. H. *J. Am. Chem. Soc.* **1997**, *119*, 3853−3860.
(9) Datta, A.; Hrovat, D. A.; Borden, W. T. *J. Am. Chem. Soc.* **2008**, *130*, 2726−2727.
(10) Karmakar, S.; Datta, A. *Angew. Chem., Int. Ed.* **2014**, *53*, 9587−9591.
(11) Karmakar, S.; Datta, A. *J. Phys. Chem. B* **2014**, *118*, 2553−2558.
(12) Liu, Y. P.; Lynch, G. C.; Truong, T. N.; Lu, D. H.; Truhlar, D. G.; Garrett, B. C. *J. Am. Chem. Soc.* **1993**, *115*, 2408−2415.
(13) Shelton, G. R.; Hrovat, D. A.; Borden, W. T. *J. Am. Chem. Soc.* **2007**, *129*, 164−168.
(14) Carpenter, B. K. *J. Am. Chem. Soc.* **1983**, *105*, 1700−1701.
(15) Whitman, D. W.; Carpenter, B. K. *J. Am. Chem. Soc.* **1982**, *104*, 6473−6474.
(16) Gerbig, D.; Ley, D.; Schreiner, P. R. *Org. Lett.* **2011**, *13*, 3526−3529.
(17) Karmakar, S.; Datta, A. *J. Phys. Chem. B* **2016**, *120*, 945−950.
(18) Borden, W. T. *WIREs Comput. Mol. Sci.* **2016**, *6*, 20−46.
(19) Truong, T. N.; Truhlar, D. G. *J. Chem. Phys.* **1990**, *93*, 1761−1769.
(20) Ley, D.; Gerbig, D.; Schreiner, P. R. *Org. Biomol. Chem.* **2012**, *10*, 3781−3790.
(21) Schreiner, P. R.; Reisenauer, H. P.; Ley, D.; Gerbig, D.; Wu, C.-H.; Allen, W. D. *Science* **2011**, *332*, 1300−1303.
(22) Ley, D.; Gerbig, D.; Schreiner, P. R. *Chem. Sci.* **2013**, *4*, 677−684.
(23) Kozuch, S.; Zhang, X.; Hrovat, D. A.; Borden, W. T. *J. Am. Chem. Soc.* **2013**, *135*, 17274−17277.
(24) Schreiner, P. R.; Wagner, J. P.; Reisenauer, H. P.; Gerbig, D.; Ley, D.; Sarka, J. n.; Császár, A. G.; Vaughn, A.; Allen, W. D. *J. Am. Chem. Soc.* **2015**, *137*, 7828−7834.
(25) Zhang, X.; Hrovat, D. A.; Borden, W. T. *Org. Lett.* **2010**, *12*, 2798−2801.
(26) McNamara, O. A.; Maguire, A. R. *Tetrahedron* **2011**, *67*, 9−40.
(27) Huisgen, R.; Dahmen, A.; Huber, H. *J. Am. Chem. Soc.* **1967**, *89*, 7130−7131.
(28) Nicolaou, K.; Petasis, N.; Uenishi, J.; Zipkin, R. *J. Am. Chem. Soc.* **1982**, *104*, 5557−5558.
(29) Nicolaou, K.; Petasis, N.; Zipkin, R.; Uenishi, J. *J. Am. Chem. Soc.* **1982**, *104*, 5555−5557.
(30) Miller, A. K.; Trauner, D. *Angew. Chem., Int. Ed.* **2005**, *44*, 4602−4606.
(31) Kurosawa, K.; Takahashi, K.; Tsuda, E. *J. Antibiot.* **2001**, *54*, 541−547.
(32) Moses, J. E.; Baldwin, J. E.; Marquez, R.; Adlington, R. M.; Cowley, A. R. *Org. Lett.* **2002**, *4*, 3731−3734.
(33) Manzo, E.; Ciavatta, M. L.; Gavagnin, M.; Mollo, E.; Wahidulla, S.; Cimino, G. *Tetrahedron Lett.* **2005**, *46*, 465−468.
(34) Wagner, P. J. *Acc. Chem. Res.* **2001**, *34*, 1−8.
(35) Assante, G.; Dallavalle, S.; Martino, P. A. *J. Antibiot.* **2013**, *66*, 43.
(36) Siengalewicz, P.; Mulzer, J.; Rinner, U. *Eur. J. Org. Chem.* **2011**, *2011*, 7041−7055.
(37) Lee, C.; Yang, W.; Parr, R. G. *Phys. Rev. B: Condens. Matter Mater. Phys.* **1988**, *37*, 785.
(38) Becke, A. D. *J. Chem. Phys.* **1993**, *98*, 5648−5652.
(39) Elango, M.; Subramanian, V. *J. Phys. Chem. A* **2005**, *109*, 11870−11877.
(40) Guner, V.; Khuong, K. S.; Leach, A. G.; Lee, P. S.; Bartberger, M. D.; Houk, K. *J. Phys. Chem. A* **2003**, *107*, 11445−11459.
(41) Lecea, B.; Arrieta, A.; Cossío, F. P. *J. Org. Chem.* **2005**, *70*, 1035−1041.
(42) Tantillo, D. J.; Lee, J. K. *Annu. Rep. Prog. Chem., Sect. B: Org. Chem.* **2009**, *105*, 285−309.
(43) Fry, A. J. *Tetrahedron* **2008**, *64*, 2101−2103.
(44) Hess, B. A.; Baldwin, J. E. *J. Org. Chem.* **2002**, *67*, 6025−6033.
(45) Clark, T.; Chandrasekhar, J.; Spitznagel, G. W.; Schleyer, P. V. R. *J. Comput. Chem.* **1983**, *4*, 294−301.
(46) Truhlar, D. G.; Garrett, B. C. *Annu. Rev. Phys. Chem.* **1984**, *35*, 159−189.
(47) Hu, W.-P.; Liu, Y.-P.; Truhlar, D. G. *J. Chem. Soc., Faraday Trans.* **1994**, *90*, 1715−1725.
(48) Fernandez-Ramos, A.; Ellingson, B. A.; Garrett, B. C.; Truhlar, D. G. *Reviews in computational chemistry* **2007**, *23*, 125.
(49) Zheng, J.; Zhang, S.; Corchado, J. C.; Chuang, Y. Y.; Coitino, E. L.; Ellingson, B. A.; Truhlar, D. G. *GAUSSRATE*, version 2010; University of Minnesota: Minneapolis, MN, 2010.

DOI: 10.1021/acs.joc.6b02759
J. Org. Chem. 2017, 82, 1558−1566

(50) Frisch, M. J.; Trucks, G. W.; Schlegel, H. B.; Scuseria, G. E.; Robb, M. A.; Cheeseman, J. R.; Montgomery, J. A.; Vreven, J. T.; Kudin, K. N.; Burant, J. C. et al. *Gaussian 09*, Revision A. 01; Gaussian, Inc: Wallingford, CT, 2009.
(51) Zheng, J.; Zhang, S.; Lynch, B. J.; Corchado, J. C.; Chuang, Y. Y.; Fast, P. L.; Hu, W. P.; Liu, Y. P.; Lynch, G. C.; Nguyen, K. A. et al. *POLYRATE*, version 2010; University of Minnesota: Minneapolis, MN, 2010.
(52) González-Lafont, A.; Villa, J.; Lluch, J. M.; Bertrán, J.; Steckler, R.; Truhlar, D. G. *J. Phys. Chem. A* **1998**, *102*, 3420−3428.
(53) Hrovat, D. A.; Chen, J.; Houk, K.; Borden, W. T. *J. Am. Chem. Soc.* **2000**, *122*, 7456−7460.
(54) Laidler, K. J. *Chemical Kinetics*, 3rd ed.; Harper: New York, 1987.
(55) Yu, T.-Q.; Fu, Y.; Liu, L.; Guo, Q.-X. *J. Org. Chem.* **2006**, *71*, 6157−6164.

DOI: 10.1021/acs.joc.6b02759
J. Org. Chem. 2017, 82, 1558−1566